Solution and Structural Properties of Colloidal Charged Lipid A (Diphosphate) Dispersions

Chester A. Faunce and Henrich H. Paradies*

The University of Salford, Joule Physics Laboratory, Institute for Materials Science Research, Greater Manchester M5 4WT, United Kingdom

Peter Quitschau

Universität Paderborn, Fachbereich Naturwissenschaften, Institut für Technische Chemie & Verfahrenstechnik, Warburger Strasse 100, D-33095 Paderborn, Germany

Received: August 7, 2002; In Final Form: November 12, 2002

It has been possible to prepare electrostatically stabilized aqueous dispersions of lipid A (diphosphate) particles of low polydispersity at low ionic strength (1−10 mM NaCl) over a range of volume fractions of $1.5 \times 10^{-4} < \phi < 5.75 \times 10^{-4}$ (25 °C). These suspensions have been characterized by transmission electron microscopy, light scattering, osmotic pressure measurements, and small-angle X-ray scattering experiments at 25 °C. All four measurements yielded independent values for particle sizes, weighted-average molecular weights, number-average molecular weights, and particle surface charge. The mean values obtained are $\bar{R} = 37.59 \pm 0.75$ nm, $\overline{R_g} = 24.89 \pm 0.88$ nm, $\overline{M_w} = (10.55 \pm 0.78) \times 10^6$ g/mol, $\overline{M_n} = (9.81 \pm 0.90) \times 10^6$ g/mol, and the effective surface charge $Z^* = (756 \pm 85)$. Very good experimental agreement is found for the directly measured osmotic pressure values and those determined from light scattering and small-angle X-ray scattering measurements as a function of volume fraction, ϕ, by applying liquid-state theory models. Using the particle parameters for the lipid A (diphosphate) system as determined, the scattering functions and the osmotic pressures can be compared as a function of volume fraction with no adjustable parameters. The ordering of lipid A in solution revealed a body-centered cubic (bcc) type lattice ($a = 36.14$ nm) at volume fractions of $3.75 \times 10^{-4} < \phi < 4.15 \times 10^{-4}$, whereas at volume fractions of $4.15 \times 10^{-4} < \phi < 5.75 \times 10^{-4}$ in the presence of 1.0 mM NaCl a face-centered cubic (fcc) lattice type ($a = 57.25$ nm) was observed. Small-angle X-ray scattering experiments also indicate the presence of long-ranged order at 1.0 mM or at 10.0 mM NaCl for lipid A dispersions of $3.75 \times 10^{-4} < \phi < 5.75 \times 10^{-4}$.

I. Introduction

Monodispersed colloidal particles, having a spherical symmetric interaction potential, are known to crystallize as colloidal crystals in several crystal structures depending particularly on the range of their mutual interaction potential.[1] A further consequence of the size of the colloidal particles is that the crystalline structures they form have a very low elastic modulus compared to that of molecular crystals. Although liquidlike ordered colloidal suspensions resemble molecular fluids in several aspects, there are many differences between colloidal and ordinary fluids. Ordinary liquids show a steep short-ranged repulsive potential and long-range weak attraction, which limits the fluid state to a rather narrow density range. However, high packing density is necessary to produce the well-known short-range order, where the first neighbors are generally located at a distance of one atomic or molecular diameter. However, dispersions of particles having long-range repulsive interactions undergo order−disorder transitions that are less visible with decreasing volume fractions. The presence of van der Waals and/or electric forces permits the colloidal particles to interact over much longer distances than short-range excluded-volume interactions experienced by hard spheres.[6] If the repulsion between the particles is large, then this transition from liquidlike to solidlike behavior also occurs over a very narrow range of volume fraction, ϕ, even as low as $\phi \leq 2.5 \times 10^{-4}$, as has been shown recently for charged silica dispersions[2] and for a lipid A modification.[3] As the volume fraction is increased, these dispersions change from liquidlike to soft solidlike and finally become solidlike.[4] Moreover, crystalline colloidal arrays are mesoscopically periodic fluid materials that efficiently diffract light according to the Bragg conditions. These crystalline materials consist of arrays of colloidal particles that self-assemble in solution into either face-centered cubic (fcc) or body-centered-cubic (bcc) crystalline arrays[5] having lattice constants in the mesoscale range of 20−500 nm. The particle size is nearly uniform and typically around 0.1 μm. Iridescence, due to strong Bragg scattering of visible light by the crystal lattice, gives visual evidence of long-range order, and this has also been observed for lipid A suspensions.[3]

The self-organization of charged particles such as lipid A (diphosphate), including their analogues, and their effects on complex fluids have received little attention. Moreover, charged particle dispersions in the nanosize regime such as lipid A (diphosphate) can influence the system stability by segregating to domains near large uncharged colloidal particles, especially in systems with small to large spheres and large size asymmetry.[6,7]

Lipopolysaccharides (LPS) or gram-negative endotoxins from the surface of gram-negative bacteria are the major component

* Corresponding author. E-mail: Hparadies@aol.com. Phone: (049)-2371-566-137. Fax: (049)-2371-566-346.

10.1021/jp0218138 CCC: $25.00
Published on Web 02/14/2003

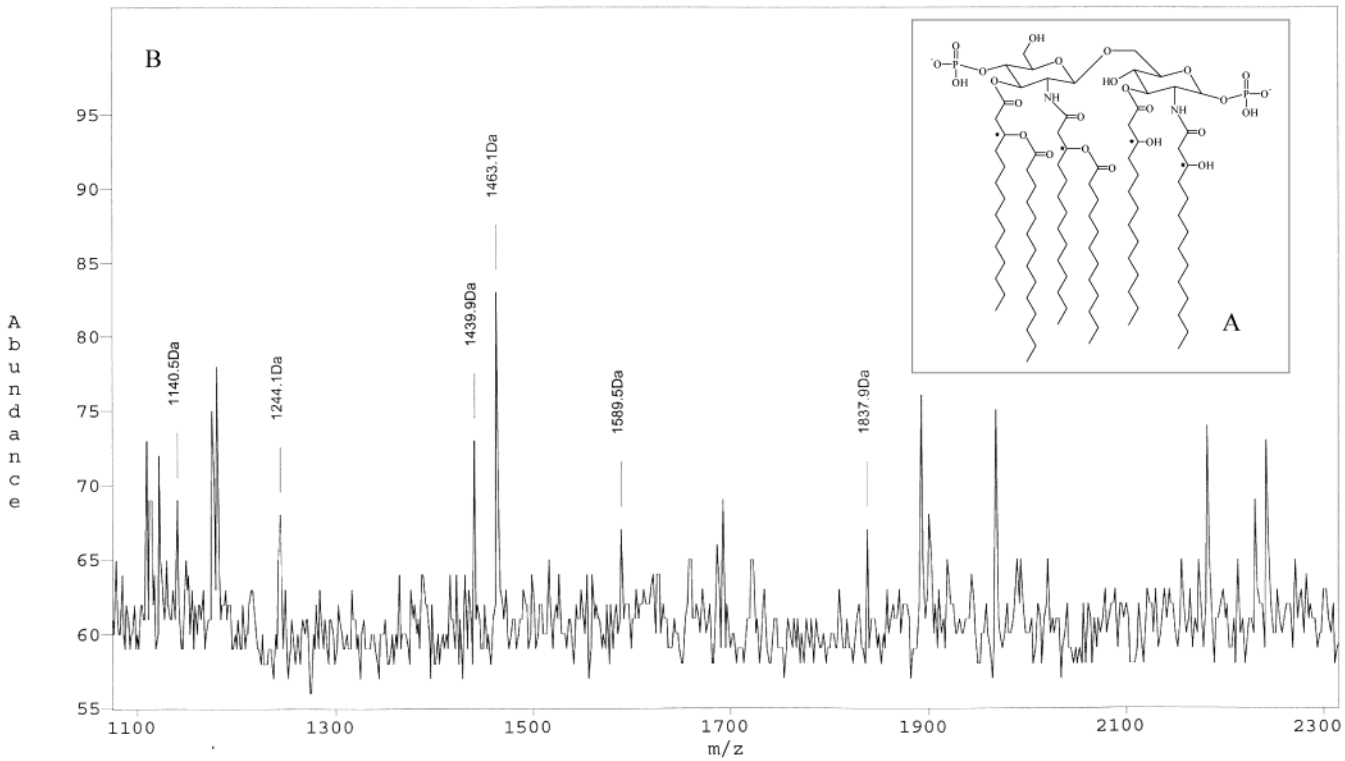

Figure 1. (A) Chemical structure of lipid A (diphosphate). Chemically, lipid A (diphosphate) from *E. coli* consists of a 1,4-diphosphorylated β-1,6-linked D-glucosamine disaccharide with four residues of amide and esterified (*R*)-3-hydroxy fatty acids. (B) High-resolution MALDI-TOF-MS spectrum of lipid A (diphosphate). All values of $[M + H]^+$ given are the average mass rounded to the nearest whole number for singly charged deprotonated lipid A (diphosphate) molecules.

of the outer leaflet of the outer membrane.[8] The conserved component of LPS is lipid A, which is linked to a core of oligopolysaccharides. Lipid A in its diphosphate form consists of a β-1,6-linked D-glucosamine disaccharide carrying six saturated fatty acid residues and two negatively charged phosphates at the reducing and nonreducing ends of the glucosamine (Figure 1A). There is considerable interest in understanding the properties of LPS and pyrophosphorylated lipid A because their release in the course of bacterial infections is the cause of septic shock in humans.[9] Recently, Kotra et al.[10] visualized the LPS molecule by means of atomic force microscopy, revealing the highest-resolution images of any bacterium to date of 50-Å lateral and 5-Å vertical resolution. The physical structure of lipid A is of considerable importance, with a variety of applications[11] (e.g., vaccine therapy,[12] LPS inhibitor binding,[13] chain-length-dependent agglutination of oligosaccharide clustering by multivalent anion binding, endotoxin inhibitors,[14] as templates for the production of nanosized materials,[15] and in biomineralization[16]). Therefore, the solution behavior of lipid A is of considerable interest in many respects. To study this large-particle system, light-scattering (LS) experiments are generally acceptable. However, because of the size, polydispersity, and index of refraction of this material in aqueous solutions, multiple scattering effects can often arise at volume fractions as low as 1×10^{-3}. Recently, it has been possible to circumvent this problem, and the lipid A system has been characterized under deionized conditions.[3] Moreover, the small size (21.5−47.5 nm) of the previous lipid A aggregate[3,17] and the present one, which contains *only* the diphosphate (Figure 1), makes it possible to perform direct measurements of the osmotic pressure (π). The obtained results of the osmotic pressure experiments can be compared with those from LS, SAXS, and SANS experiments using calculated and directly measured structure factors $S(Q)$. The appearance of highly ordered regions resembling crystal-like structures as a function of volume fraction enables us to study the structural and thermodynamic properties in much more detail. Much is known about predicting the various phases of such systems, typically, fluid, body-centered cubic (bcc), face-centered cubic (fcc), and quasi-crystalline as a function of volume fraction, temperature (melting), and for comparing their structures with those in real systems.[18,19] Therefore, it is interesting to examine the lipid A system in more detail since no crystalline ordering was found from the onset for these suspensions, all of which are transparent to light and have a low index of refraction.

Three independent methods have been used to investigate the thermodynamic and structural properties of this lipid A system: (i) light scattering (LS), (ii) osmotic pressure (π) measurements, and (iii) small-angle X-ray scattering (SAXS). All three techniques yield information on the structural behavior of the suspension as a function of volume fraction ($1.5 \times 10^{-4} < \phi < 5.75 \times 10^{-4}$) in the presence of low concentrations of salt (1 mM < [NaCl] < 10 mM) at 25 °C. In addition, the results that are obtained can be interpreted according to existing models of liquid-state theory. One can infer from the combined experimental LS and SAXS data that there are at least two ordered structures of lipid A in aqueous solutions whose presence depends mainly on their volume fractions ϕ.

II. Experimental Section

A. Materials. Diphosphorylated lipid A was extracted from the *E. coli* bacteria (K 12) by 0.05 M sodium acetate in the presence of 0.001 M acetic acid or citrate (1 mM) at 4 °C and subsequently purified by HPLC (Beckman Gold) using a linear gradient for elution containing 0.001 M acetic acid and 0.015 M ammonium acetate.[3,17] The flow rate was generally 1.5 mL/h. Peaks were monitored by a differential refractive index

detector coupled to a LS apparatus, which calculates the weighted-average molecular weights of the desired peaks, as well as through their angle dependency (five different angles), the weighted-average radius of gyration, and their dispersion. Size-exclusion chromatography (SEC) was performed as described previously.[20] The average weighted molecular weights obtained by these techniques are $\overline{M}w = (10.81 \pm 0.96) \times 10^6$ g/mol (light -scattering detector) and $\overline{M}_w = (11.41 \pm 0.96) \times 10^6$ g/mol (SEC). The material was analyzed by MALDI-TOF-MS[3], electron-spray/MS, and GC/MS. Figure 1B shows a mass spectrum of the lipid A material that has been used throughout the physical measurements. Elemental analysis and phosphate content measurements were performed as described in refs 21 and 22 using lyophilized lipid A material. The lipid A specimens investigated by SEM for the determination of the particle-size distribution were also analyzed for phosphorus content through EDX attached to the SEM (JEOL 6400).

The pure lipid A material that was obtained was dialyzed against several changes of 0.1 M NaCl at 20 °C: Any particulate matter was removed by filtration through a Millipore filter (exclusion particle-size diameter 2.0 μm). The sodium salt of lipid A (500 μg/mL) was diluted until a concentration of 100 μg/mL was reached. Centrifugation of this solution at 20 000*g* (Beckman Centrifuge, J 52 B) for 20 min resulted in a slightly iridescent solution. However, this solution is very susceptible to changes in ionic strength and/or concentration, for example, through ultrafiltration, which can result in amorphous material that precipitates completely after 1−5 h. The solution was heated briefly to 75 °C for 1 min, rapidly cooled to 20 °C, and washed using a tangential ultrafiltration module (Schleicher and Schüll) that removes water from the sol and replaces it with deionized water, thus continuously reducing the ionic strength of the sol. Using this procedure, a batch of lipid A was washed until the water leaving the system has a conductivity close to that of the deionized water used in the tangential ultrafiltration module. At this stage, the batch of lipid A was divided into two portions. One portion was concentrated to a volume fraction of $\phi = 1.2 \times 10^{-2}$ whereas the other portion was diluted to a volume fraction of $\phi = 1.2 \times 10^{-3}$, both portions having an ionic strength of 2.5×10^{-5} M. This procedure permits the examination of two systems of lipid A that differ only in volume fraction.

The stock solutions of lipid A suspensions were then dialyzed (Medicell International, Ltd., Visking Tubing, London) several times against purified water that had been deionized by using cation- and anion-exchange resins (Millipore) and further purified by a Milli-Q reagent-grade system from Millipore. After several dialysis changes, the suspensions were passed through a mixed bed of cation- and anion-exchange resins from BioRad (Munich, Germany, AG 501-X8, 500 mesh) for at least a week prior to crystallization at 4 °C or were stored over the resins for different periods of time (e.g., 1, 2, and up to 6 weeks before the onset of crystallization at temperatures between 8 and 20 °C). The ion-exchange resins from BioRad were treated with the same Millipore water before the exchange experiments (e.g., Na^+ to H^+) were performed. In essence, a fixed quantity of water was used, and the effluent was recirculated. This procedure ensured that the equilibrium system conditions (e.g., ionic strength and pH) were always maintained. These solutions were all transparent. The concentration of lipid A was determined by weighing a sample before and after drying in an oven at 100 °C under a stream of N_2 (99.99%) for 2 h. The conversion of units from mass fraction to concentration in μg of lipid A/liter, *c*, and volume fraction, ϕ, was made by assuming a density of dry lipid A of 1.37 ± 0.072 g/cm^3 as determined from density measurements using a Paar densitometer (Graz, Austria) and gradient centrifugation.[3] Similar values were reported by Hayter et al.,[23] Hannecart-Pokorni et al.,[24] and Shands and Chun.[25]

B. Scattering. Static light-scattering (LS) and quasi-elastic light-scattering (QELS) experiments were performed using an instrument described previously.[3] The light source was a polarized laser beam (NEC-Laser, 50 mW He−Ne) with a wavelength of $\lambda_0 = 623.8$ nm. The incident beam was vertically polarized, and the intensity was adjusted by a combination of neutral density filters, including a half-wave plate and a polarizer, to achieve a maximum amplitude within the linear range of the photomultiplier response. QELS experiments for the dilute suspensions of lipid A ($1.5 \times 10^{-4} \leq \phi \leq 2.5 \times 10^{-4}$) were performed at scattering angles of $10° \leq \theta \leq 125°$ to determine the apparent hydrodynamic radius $\overline{R}_{ap}$ in the presence of 1−10 mM NaCl. A pinhole (50 μm) on the detector area was used to define one coherent area.[26] The experimental diffusion coefficient, $D_{exp}(Q)$, was obtained from the first cumulant $\Gamma^{(1)}_{exp}(Q)$, which provided the values of the average free-particle diffusion coefficient $D^0(2\bar{a})$ of the suspension of noninteracting homogeneous spheres of diameter $2\bar{a}$ (section III.C). The average hydrodynamic radius $\overline{R}_{ap}$ was calculated according to the Stokes−Einstein relation. The obtained $\overline{R}_{ap}$ for the dilute regime was compared with those measured by TEM. Moreover, the normalized second cumulant, $[\{\Gamma^2_{exp}(0)\}/\{\Gamma^1_{exp}\}(0)]^2$, was used as an additional measure of the degree of polydispersity $\overline{\rho_{QELS}}^3$.

Static light-scattering (LS) measurements from dilute suspensions of lipid A of $\phi = 1.0 \times 10^{-4}$ to 3.5×10^{-4} were performed at *Q* values between 8.0×10^{-3} and 3.5×10^{-2} nm^{-1} on the same goniometer to determine the rms radii of gyration $(\overline{R}^2_g)^{1/2}$ from the angular dependence of the mean scattering intensity, *I*(*Q*), according to Guinier.[27] The alignment of the apparatus, particularly for the angular dependence of the scattered intensity, was tested using an aqueous suspension of well-characterized colloidal polystyrene particles (Sigma-Aldrich), and the form factor, *P*(*Q*), was verified with Mie scattering theory. Average intensities were obtained from 20 individual runs at each scattering angle, and *I*(*Q*) was corrected for variations in the scattering volume.

For determinations of *S*(*Q*) at various concentrations of the lipid A suspensions, the samples were diluted from the dialyzed stock solution (0.1 mg/mL lipid A*)* to the appropriate particle concentration and ionic strength and subsequently filtered through 1.0-mm prerinsed cellulose acetate filters (Schüll, FRG) and finally through Millipore filters into the light-scattering cells (25 °C). Scattering intensities were measured for *S*(*Q*) in the above-mentioned *Q* range in 0.1° steps for angles around the first intensity maximum and in 2.5° steps for higher angles. The accessible range was limited to the low volume-fraction range of lipid A to avoid Bragg reflections, which would superimpose on the scattering from the coexisting liquid phase because at higher concentrations, $\phi_c > 3.5 \times 10^{-3}$, the samples of lipid A crystallize into colloidal crystals of sizes up to 200 mm.[17] The absorbance at 556 nm due to scattering was 0.15 for the lipid A suspensions.

Small-angle X-ray scattering (SAXS) experiments, including data handling and processing, were performed as described previously.[28] Data were recorded for *Q* values as low as 0.02 nm^{-1} (Cu Kα radiation ($\lambda = 0.154$ nm)). The beam was Kα/Kβ filtered and focused in horizontal and vertical directions by total reflection from curved Franks mirrors. The liquid samples were placed in 1.5-mm-thick cell holders surrounded by a

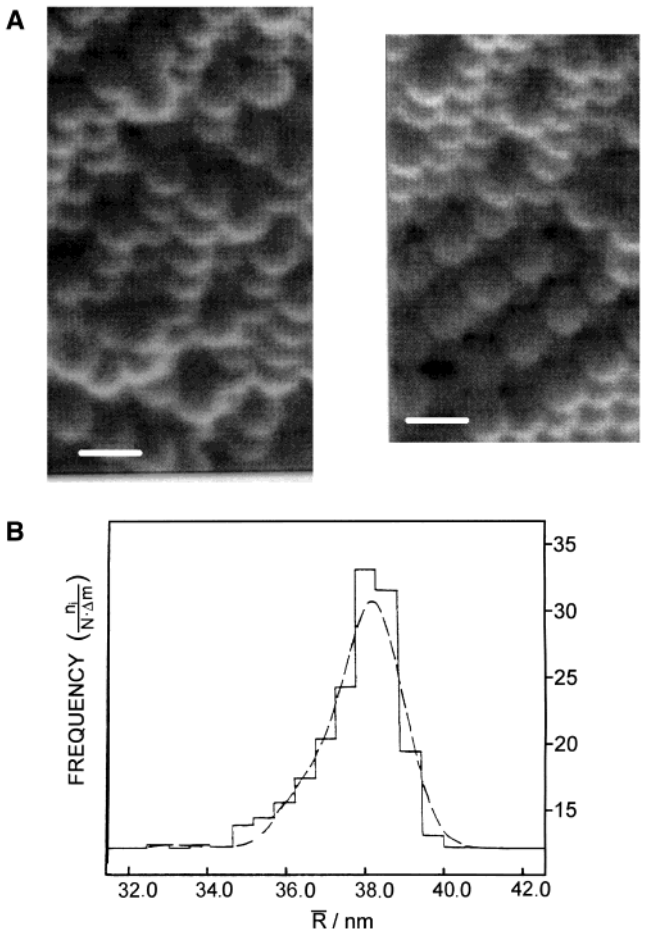

Figure 2. (A) SEM electron micrograph of lipid A (diphosphate) aggregates at volume fractions of $\phi = 2.5 \times 10^{-4}$ (left) and 3.75×10^{-4} (right). The size bar is 100 nm. (B) Size distribution of lipid A aggregates obtained by transmission electron microscopy. Full line histogram, original data; dashed line, smoothed distribution calculated from the histogram with the average radius of $\bar{R} = 37.59$ nm and a polydispersity of $r = 8.1\%$.

Kepton film. The scattering vector Q varied from 0.3 to 3.0 nm^{-1}, and the dQ/Q resolution was on the order of 0.04.

Particle-size distributions were characterized by imaging the particles at a voltage of 20 kV using a scanning electron microscope (JEOL 6400) and at a voltage of 200 kV using a transmission microscope (JEOL 3010). They were calibrated using a Pt grid with 2180 lines/mm. Different batches of lipid A preparations exhibit the same chemical composition and yield the same size distribution. After freeze drying, no differences were experienced in the size distribution between samples between those that had been covered with a carbon film and those that had not. The particle diameters of individual particles were determined from the images (Figure 2A). The smoothed distribution from a sample of 625 particles yields an average radius $\bar{R}$ of 34.75 ± 0.75 nm, and the normalized variance $\overline{\rho_{TEM}} = (\overline{R^2}/\bar{R}^2 - 1)^{1/2}$ was evaluated as 8.7 ± 0.8 (Figure 2B).

C. Osmotic Pressure Measurements. Measurements were made on solutions of lipid A using a Knauer membrane osmometer (Berlin, FRG), applying a 20 000 MW (Visking, UK) membrane, which measures pressures between 1.2 and 4000 Pa. A small volume of lipid A of known concentration was placed on one side of the membrane, and on the other side of the membrane was water that had been collected during the concentration process. It is important to note that we used the water obtained during this process of concentrating the lipid A solution both to dilute the concentrated solution and for the reference cell. It has been assumed that since the water used in the dilution of the lipid A sample contains the same foreign ions as those in the osmotic pressure experiment they must be in equilibrium. Moreover, it is important that for all measurements a single preparation of lipid A of each concentration was prepared and used throughout.

D. Apparent Weighted-Average Molecular Weights. Extrapolating the light-scattering intensity and osmotic pressure to infinite dilution (no interactions) yields the weight-average molecular weight M_w and the number-average molecular weight M_n. M_w is given by

$$\frac{1}{M_w} = \lim_{c,Q\to 0} \frac{K'cI_{toluene}(Q)}{I_p(Q)} \tag{1}$$

where I_P and $I_{toluene}$ are the intensities scattered by the lipid A suspension and the reference liquid toluene, respectively. K' is defined as

$$K' = 4\pi^2\left(\frac{dn}{dc}\right)_\mu^2\left(\frac{1}{N_A\lambda^4}\right)\left(\frac{n_{toluene}^2}{R_{toluene}}\right) \tag{2}$$

where $n_{toluene}$ and $R_{toluene}$ are the index of refraction and the Rayleigh factor for toluene, respectively. The constant K' was 2.39×10^{-6} mol L/g^2, and $(dn/dc)_\mu = 0.138$ mL/g, as determined on a Brice Phoenix model 2000 VIRTIS differential refractometer (25 °C).[29] The calibration of the instrument was performed with solutions of KCl of known concentrations. The osmotic pressure measurements in the limit of weak interactions, M_n, is given by eq 3:

$$\frac{1}{M_n} = \lim_{c\to 0} \frac{\pi}{N_A k_b T c} \tag{3}$$

III. Theory

A. Monodisperse System. The experimental data were analyzed according to liquid-state theory since there is a close relationship between colloidal suspensions and classical liquids.[30] The normalized measured scattered intensity of a light beam by a suspension of monodisperse spherical particles is

$$I_p(Q) = K\varnothing a^6 P(Q)\, S(Q) \tag{4}$$

where $S(Q)$ is the structure factor and a is the radius of this particle. $S(Q)$ can be evaluated as a function of ϕ. Here, K is a constant depending on the optical properties of the particle and the solvent. The quantity $Q = |Q|$ is related to the scattering angle θ by $Q = (4\pi/\lambda)\sin(\theta/2)$, where λ is the wavelength in the suspension and $P(Q)$, the particle form factor, is the square of the normalized scattering amplitude $P(Q) = f^2(Qa)$, with a as the particle radius. The structure factor $S(Q)$ for a system of interacting particles is

$$S(Q) = 1 + \frac{4\pi\rho}{Q}\int_0^\infty [g(r) - 1] r \sin Qr\, dr \tag{5}$$

where $g(r)$ is the pair distribution function, $\rho = c/M$ is the particle number density, and r is the center-to-center distance between particles. For a system of monodisperse particles that interact through strongly repulsive forces, $S(Q)$ is related to the osmotic compressibility and isothermal compressibility of the

liquid in the long-wavelength limit ($Q \rightarrow 0$) according to[30]

$$S(Q=0) = \frac{k_b T}{(\partial\pi/\partial\rho)_T} \tag{6}$$

where π is the osmotic pressure. In case of $S(Q=0)$, eq 6 can be rewritten to determine $\pi(\phi)$ as

$$\pi(\phi) = \frac{3k_b T}{4\pi a^3}\int_0^\phi \frac{1}{S(Q=0,\phi)}\,\mathrm{d}\phi \tag{7}$$

For a monodisperse system, $S(0)$ and the osmotic pressure π can be compared directly.

B. Polydisperse Systems. The interpretation of scattering results for colloidal suspensions is influenced by the polydispersity in size, shape, and charge or by the refractive index. In the absence of interactions, it can be treated using the integral form of eq 8:[30]

$$I_p(Q) = K\sum_{ij}\sqrt{c_i c_j M_i M_j f(Qa_i)\, f(Qa_j)\, S_{ij}(Q)} \tag{8}$$

where a_i, $M_i \propto a_i^3$, and $c_i = \rho_i M_i$ are the average radius, molecular weight, and weight-average molecular weight of species i and the $S_{ij}(Q)$ are the partial structure factors. In the limit of systems of weakly interacting particles, $S_{ij}(Q) = \delta_{ij}$, so eq 9 holds:

$$I_{p,o}(Q) = K\sum_i \rho_i M_i^2 P_i(Q) = K\int_0^\infty \rho(x)\, M^2(x)\, f^2(Qx)\,\mathrm{d}x \tag{9}$$

$\rho(x)\,\mathrm{d}x$ represents the number of particles per unit volume with a radius between x and $x + \mathrm{d}x$. In dilute systems, the polydispersity can generally be treated using the integral form of eq 9, assuming a Gaussian distribution for $\rho(x)$:

$$\rho(x) \propto \exp\left[-\frac{1}{2}\left(\frac{x-a}{\sigma}\right)^2\right] \tag{10}$$

where a is the average size of the particle and σ is the width of the distribution. We also tried other distribution functions, particularly the Shultz distribution. The differences between the Gaussian distribution and the Shultz distribution are the Shultz's skew symmetry toward larger particle sizes and approach toward a Gaussian distribution for small values of the standard deviation. Although other choices for the size distribution exist, the detailed shape of this distribution for this low polydispersity was found not to be critical for our sufficiently small standard deviations for the very dilute suspension studied here. Moreover, as shown below (section IV.C) for the calculation of the structure factors, we found that a three-subcomponent system was adequate as long as the standard deviation was <0.28 within the range of our experimentally probed wavenumbers.

The expression in eq 8 has been used in the presence of interactions for polydispersed suspensions and will represented by a three-component mixture of sizes $a - \sigma$, a, and $a - \sigma$ having relative number densities of 1, 2, and 1. The equilibrium pressure, compressibility, and structural properties of $S_{ij}(Q)$ can be obtained from liquid-state theory. The height of the first peak of $S(Q)$ was calculated with the hypernetted chain approximation (HCNA) combined with the Rogers−Young closure[31] for the volume fractions of lipid A. The mixing parameter α was chosen in such a way that $\chi_T^{(f)}$ and $\chi_T^{(v)}$ computed from the fluctuation and virial expressions, respectively, coincide. The fluctuation compressibility $\chi_T^{(f)}$ was directly calculated from $S(Q=0)$ through $\chi_T^{(f)} = (\beta/n)\, S(Q=0)$, and the virial compressibility $\chi_T^{(v)} = (\partial[\beta P]/\partial n)_T^{-1}$) was obtained from the equation of state (eq 11):

$$\frac{\beta P}{n} = 1 - \frac{2\pi\beta n}{3}\int_0^\infty g(r)\,\frac{\mathrm{d}U(r)}{\mathrm{d}r} r^3\,\mathrm{d}r \tag{11}$$

Moreover, since the pair distribution function tends to the Boltzmann factor $\mathrm{e}^{-\beta U(r)}$ at zero concentration, the virial coefficient also be calculated from eq 12:

$$\chi_T^{(v)} = \int_0^\infty (1 - \mathrm{e}^{-\beta U(r)})\, 4\pi r^2\,\mathrm{d}r \tag{12}$$

Considering a primitive model description, all mutual correlations between macro-ions and the salt electrolyte ions interact through the Coulomb potential. Since we are mainly interested in the structure of the lipid A suspension, an effective one-component description without the degrees of small ions seems appropriate. The screening of the bare Coulomb interactions by the salt ions results in a potential of mean force $U(r)$ between the macro-ions that depends on the charge and number density of the macro-ions. But different structures can have different radii a_μ and a_ν and also carry different charges Z_μ and Z_ν, so with increasing polydispersity, the main peak of $\bar{S}(Q)$ is reduced in height and moves toward higher Q. For moderately polydisperse systems with interaction potentials between particles having radii of a_μ and a_ν and effective charges of Z_μ and Z_ν, the ion-averaged DLVO-like potential between particles[32] can be written as

$$U_{\mu\nu}(r) = \frac{Z_\mu Z_\nu e_0^2}{4\pi\epsilon_r\epsilon_0}\frac{e^{ka_\mu}}{1+ka_\mu}\frac{e^{ka_\nu}}{1+ka_\nu}\frac{e^{-kr}}{r}; \qquad r > a_\mu + a_\nu \tag{13}$$
$$= +\infty; \qquad r < a_\mu + a_\nu$$

with the screening constant $k = (2\mathrm{e}^2 I/\epsilon\epsilon_0 k_B T)^{1/2}$. I is the ionic strength, which includes the salt ions (I_S) and the counterions that equilibrate the colloidal charges, and Z_i is the number charge of colloid i according to

$$I = I_S + {}^1/_2\sum_i Z_i\rho_i \tag{14}$$

This multicomponent model was solved for the lipid A suspensions in the presence of 1−10 mM NaCl by applying the hypernetted chain integral equation (HNC). Larger particles contribute to the scattering intensity at low scattering angles, even if their particle number is small. Since the scattering amplitude also depends on the scattering-length distribution of the three-component sample, the compressibility of each individual sphere will contribute to $\bar{S}(\mathrm{Q})$ according to eq 15:

$$\rho k_B \chi_T = \frac{|S(0)|}{\sum_i\sum_j x_i x_j |S_{i,j}(0)|} \tag{15}$$

The parameters x_i and x_j are now the corresponding mole fractions of the subcomponents. (See eq 8 and Table 2.) It is also easy to define an effective structure factor from the intensities according to eq 16[2]

$$S_{\mathrm{eff}}(Q) = \frac{I_p(Q)}{I_{p,0}(Q)} \tag{16}$$

TABLE 1: Summary of the Physical Characterization of the Lipid A (Diphosphate) Particles Obtained in Aqueous Solutions Containing 1.0 mM NaCl for Volume Fractions of $1.5 \times 10^{-4} \leq \phi \leq 3.75 \times 10^{-4}$ at 25 °C

parameter	uncorrected size distribution	corrected size distribution	independently measured
$\bar{R}$/nm	34.50 ± 0.30	34.58 ± 0.81	
$\overline{\rho_{TEM}}$/%	7.80 ± 0.92	8.10 ± 0.60	
$\overline{R_H}$/nm (QELS)	38.83 ± 0.75	38.50 ± 0.65	38.70 ± 0.55
$\overline{a_H}$/nm (LS)	37.59 ± 0.30	37.59 ± 0.75	37.65 ± 0.78
$\overline{R_g}$/nm (LS)	24.88 ± 0.75	24.80 ± 0.75	24.88 ± 0.80
$\overline{\rho_{LS}}$/%	5.00 ± 0.70	5.00 ± 0.70	
$\overline{\rho_{QELS}}$/%	7.70 ± 0.75	7.75 ± 0.75	
[b] $\overline{M_w} \times 10^6$/g mol^{-1}	10.55 ± 0.78		10.55 ± 0.78
[c] $\overline{M_n} \times 10^6$/g mol^{-1}	9.81 ± 0.90		9.81 ± 0.90
[d] $\overline{M_w} \times 10^6$/g mol^{-1}	11.0 ± 0.85		11.0 ± 0.85

[a] The first column lists the number-average particle radius $\bar{R}$, the polydispersities $\overline{\rho_{TEM}}$, $\overline{\rho_{LS}}$, and $\overline{\rho_{QELS}}$, the radius of gyration $\overline{R_g}$, and the hydrodynamic radius $\overline{R_H}$ or $\overline{a_H}$. The second column summarizes the quantities calculated from the uncorrected size distribution with respect to the independently measured quantities, the average weight-average molecular weight $\overline{M_w}$, and the average number-average molecular weight $\overline{M_n}$, and the third column summarizes the quantities calculated from the uncorrected size distribution corrected for polydispersity with respect to the independently measured quantities. [b] LS. [c] Osmometry. [d] SEC.

TABLE 2: Size Representation of Lipid A (Diphosphate) Particles for $\sigma = 0.078$ and $\overline{2a} = 37.59$ nm in Aqueous Solutions Containing 1.0 mM NaCl (25 °C)[a]

subcomponent diameters $\overline{2a}$ (nm)	relative diameters $\overline{2a_i}/\overline{2a}$	mole fractions X_i
$\overline{2a_1} = 68.04$	0.892	0.0712
$\overline{2a_2} = 75.79$	1.008	0.8750
$\overline{2a_3} = 78.27$	1.041	0.0541

[a] The number of components in the distribution (histogram) is 3. The diameters and the mole fractions of each subcomponent are listed.

But in contrast to the monodisperse system, the compressibility $\chi_T^{(\nu)}$ is now not given by $S_{eff}(Q = 0)$. The values of $\chi_T^{(\nu)}$, S_{eff} (0), and $\pi/\rho k_B$ for a monodisperse suspension with $a = 37.50$ nm in the absence of salt are 0.0087, 0085, and 118.7; the corresponding values for a polydisperse system ($m = 3$) with $a = 37.50$ nm and $\sigma = 4.0$ nm are 0.0085, 0.0097, and 99.2, indicating that the polydispersity effects are relatively small although not negligible.

The radii a_μ and the number densities n_μ ($\mu = 1,..., n$) of the components were chosen such that the first $2m$ moments of the histogram distribution coincide with those of the original histogram distribution.[33] The scattering amplitude is then the weighted sum of the contributions of the individual components (e.g., $I(Q) \propto \bar{P}(Q)\,\bar{S}(Q)$ by analogy to the monodispersed case) since the normalized scattering intensity $I(Q)$ no longer factors into parts that depend only on single particle properties or the interparticle correlations. The quantity $\bar{P}(Q)$ is the form factor average over the size distribution, and $\bar{S}(Q)$ is the measured structure factor, which contains single-particle quantities (e.g. the normalized scattering amplitude[34]). The structure factor $S(Q)$ was obtained by normalizing the reduced intensity $I(Q)/\bar{P}(Q)$ at its highest accessible Q. To avoid arbitrary shifts in $\bar{S}(Q)$ which can propagate into erroneous effective charges, the scattering intensities were analyzed for their asymptotic behavior at large Q values, and their convergence verified by using the oscillating part of $I(Q)/\bar{P}(Q)$ at lower scattering angles.[3] Moreover, the values of $\bar{S}(Q)$ were calculated for $Z_\mu \propto a_\mu$ keeping the average charge constant.

C. QELS and Polydispersity. At low volume fractions, the hydrodynamic interactions $H_{exp}(Q)$ and the polydispersity can affect the short-time dynamics, the Stokes diffusion coefficient, $D^0(2\bar{a})$, the observed hydrodynamic radius $\overline{R_h}$, and $S(Q)$.[34] In particular, the peak height at small values of Q will be affected (eq 17):

$$\frac{D_{exp}(Q)}{D^0(\overline{2a})} = \frac{H_{exp}(Q)}{S_{exp}(Q)\,D^0(\overline{2a})} \tag{17}$$

To estimate the effect of hydrodynamic interactions on $D^0(2\bar{a})$ and $S(Q)$, we compared our experimental results with the theoretical results for $D^0(2\bar{a})/D_{exp}(Q)$ as a function of size polydispersity, $\overline{\rho_{QELS}}$. $H_{exp}(Q)$ can be obtained by combining the QELS data of $D_{exp}(Q)$ with LS measurements of $S_{exp}(Q)$ through $D_{exp}(Q) = H_{exp}(Q)/S_{exp}(Q)$. The quantity used for the normalization of $D^0(2\bar{a})$ was the Stokes diffusion coefficient taken as the mean diameter of $2\bar{a} = 75.20$ nm obtained from TEM, SAXS, and QELS by the cumulant analysis for $\phi = (1.8-2.2) \times 10^{-4}$ in the presence of 1 mM NaCl (25 °C). $D_{exp}(Q)$ was obtained from a first cumulant analysis of the autocorrelation function.[3]

IV. Results and Discussion

A. Particle Characterization and Polydispersity. The quantities obtained from LS, SAXS measurements, and from TEM and SEM were used to calculate the size distribution (Figure 2B). For the radius of gyration, the expression $\overline{R_g} = [3\overline{R^8}/(5\overline{R^6})]^{1/2}$ was used, and for the hydrodynamic radius, $\overline{R_h} = \overline{R^6}/\overline{R^5}$ was employed. Assuming that particle interactions can be treated according to eqs 4−13 for volume fractions of $1.0 \times 10^{-4} \leq \phi \leq 2.5 \times 10^{-4}$ and salinities of 1−10 mM NaCl, $I_p(Q)$ was calculated using eq 9 assuming a Gaussian distribution, $r(x)$ (eq 10), and the results were compared to the experimental values obtained from static LS, TEM, and SEM. The best fit was for an average radius of $\overline{a_h} = 37.59 \pm 0.75$ nm from the light-scattering measurements (R_g) assuming that spherical particles compared with those obtained from TEM of $\overline{R_h} = 34.50 \pm 0.30$ nm (Figure 2A). The latter were consistently lower by 8.0−9.5% and were 10.0−11.5% lower than the values determined by QELS when $\overline{R_h} = 38.83 \pm 0.50$ nm (Table 1). The best fit for the average radius of lipid A, $\bar{R}$, was 34.58 ± 0.81 nm, and the normalized variance $\bar{\rho}_{TEM} = (\overline{R^2}/\bar{R}^2 - 1)^{1/2} = 7.82 \pm 0.92\%$. The measured size distribution shows, unlike the Schultz distribution calculated with the same $\bar{R}$ and $\bar{\rho}_{TEM}$, a tail at smaller sizes of lipid A.

To estimate polydispersity effects and hydrodynamic interactions $H_{exp}(Q)$ of the dilute suspensions ($1.5 \times 10^{-4} \leq \phi \leq 2.6 \times 10^{-4}$) for QELS measurements, we compared the theoretical results (eq 17) for a monodisperse system with those for various polydispersities $\bar{\rho}_{QELS}$[35] (Figure 3). The width of the principal peak in the experimental $D^0(2\bar{a})/D_{exp}(Q)$ is consistently lower in the calculations by ~4%. However, despite the lack of precise quantitative agreement, the overall trends are well documented by the lipid A model (e.g., the increase and the shift toward larger Q values of the principal peak on increasing ϕ due to an increase in interparticle correlations). The polydispersity is more pronounced at low Q, where it shows the initial decay of the field autocorrelation function by producing a substantially larger

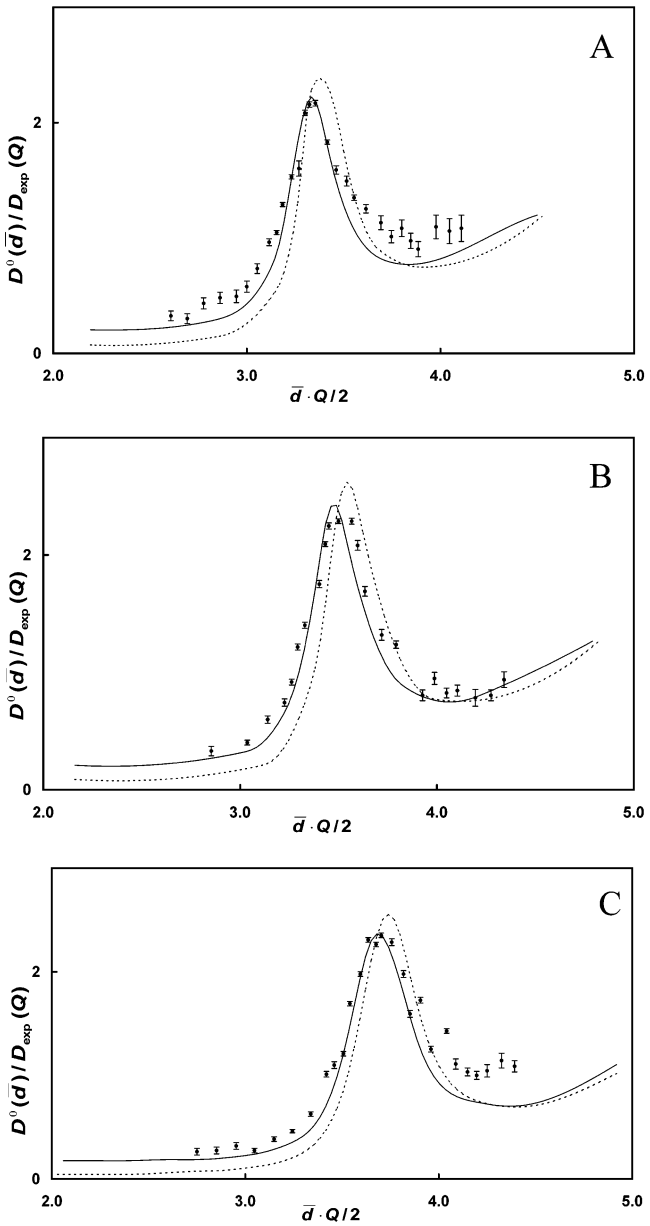

Figure 3. Normalized measured diffusion coefficient $D^0(2\bar{a})/D_{exp}(Q)$ as a function of $2\bar{a}Q$. Comparison of the QELS measurements (- -) with the theoretical results for volume fractions of $\phi = 1.8 \times 10^{-4}$ (A), 2.20×10^{-4} (B), and 2.20×10^{-4} (C) assuming a size polydispersity of $\bar{\rho} = 7.8\%$ (—) and $\bar{\rho} = 0$ (- -). $D^0(2\bar{a}) = k_BT/3\pi\eta 2\bar{a}$, with $2\bar{a} = 75.20$ nm.

$D_{exp}(Q)$ relative to that of the monodisperse suspension. The origin of this effect is the increase in $H_{exp}(Q)$ at low Q. On increasing ϕ (Figure 3), $H_{exp}(Q)$ is overcompensated by a larger decrease in $S_{exp}(Q)$. It can be inferred from the reasonable agreement between theory and experiment and the relatively low standard deviation of 0.09 obtained from the cumulant analysis that the hydrodynamic interactions are not severe because $H_{exp}/H^0_{exp}(Q) \approx 1$.

The average radius of gyration $\overline{R_g}$ was obtained from the angular dependence of the scattered light ($25° < \theta < 135°$) for suspensions of lipid A in 1.0 mM, and 10.0 mM NaCl and yielded values of $\overline{R_g} = 24.88 \pm 0.80$ and 24.80 ± 0.75 nm.

It is not unusual for particle sizes determined from TEM to be smaller than the ones obtained by QELS, LS, and SAXS or SANS scattering methods because of the shrinkage of the hydrated particles caused by the exposure to the electron beam

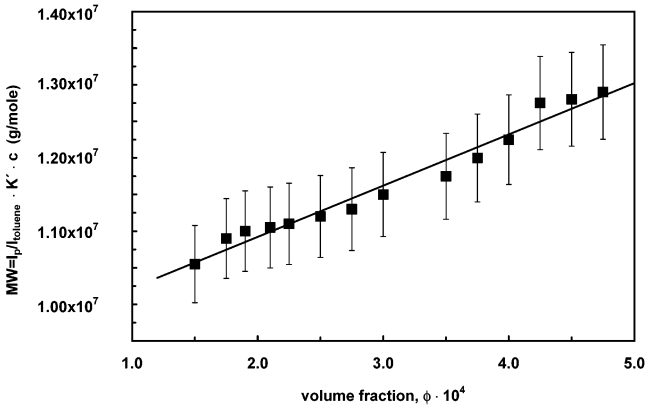

Figure 4. Molecular weight determination of lipid A (diphosphate) dispersions by static light-scattering experiments at $Q = 2.50 \times 10^{-2}$ nm (25°C) in the presence of 1.0 mM NaCl.

as well as by errors in the calibration of the electron micrographs. Thus, $\overline{R_h}$ when measured by QELS is expected to be somewhat larger than the actual particle radius because of bound water molecules at the surface of the particle. However, we cannot exclude the possibility that the differences between the radii of TEM and static light scattering could be attributed to the polydispersity of the system. The particle polydispersity, $\bar{\rho}$, can be used to decide whether to treat the system as a one-component system ($r < 5\%$). Accordingly, we calculate for the TEM results a value of 6.4% for $\bar{\rho}$, which is not inconsistent with 6.5% found from LS measurements and 7.8% found from QELS. Similar values were obtained for a Shultz distribution (6.4%) taken from the SAXS, QELS, and LS experiments. It appears that a higher degree of polydispersity can in fact be accepted for this charged-particle system. Furthermore, the TEM electron micrographs may give the false impression that a Gaussian distribution is appropriate. Indeed, the size distribution could have been of log-normal form, with a tail extending to smaller particle sizes even though we could not detect any significant number of smaller particles. If this were the case, the particle-size distribution parameter could still be higher than $8.7 \pm 0.6\%$. Applying a log-normal distribution of the particle-size polydispersity recalculated from the M_w distribution affords a value of $8.5 \pm 0.7\%$.

B. Molecular Weights. The weight-average molecular weight, M_w, for the volume fraction in the range of $1.5 \times 10^{-4} \leq \phi \leq 3.75 \times 10^{-4}$ was determined from eq 1 in the presence of 1.0 mM NaCl or 10 mM NaCl, respectively (Figure 4) The plot of $(I_P/K'cI_{toluene})$ versus ϕ reveals a slightly positive slope that is almost independent of the range of the volume fraction studied and yields, after extrapolation to $\phi = 0$, $M_w = (10.55 \pm 0.78) \times 10^6$ g/mol (Table 1). One would expect that in an electrostatically stable system particle interactions would decrease with increasing ionic strength at a given volume fraction because of the reduced particle interactions at low salt concentration and that the osmotic pressure would decrease as a function of increasing ionic strength. Thus, eq 7 will satisfy the experimental conditions reasonably well and does not affect the evaluation of the apparent weight-average molecular weight as a function of ϕ.

Similarly, the number-average molecular weight M_n, according to eq 3, was determined for both ionic strengths at volume fractions of $1.8 \times 10^{-4} < \phi < 3.75 \times 10^{-4}$ by plotting π/c as a function of c ($\phi = v_2c$, with c in g/cm^3 and v_2 the determined partial specific volume) and extrapolating to $c \rightarrow 0$, yielding values of $(9.81 \pm 0.90) \times 10^6$ g/mol and $(9.86 \pm 0.90) \times 10^6$ g/mol, respectively (Figure 5). M_n is normally lower than M_w,

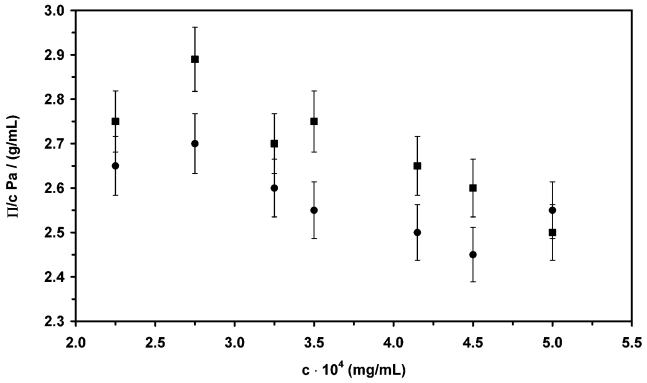

Figure 5. Molecular weight determination of lipid A (diphosphate) dispersions from osmotic pressure measurements and eq 3 at different ionic strengths: (■) 1.0 mM NaCl, (●) 10.0 mM NaCl.

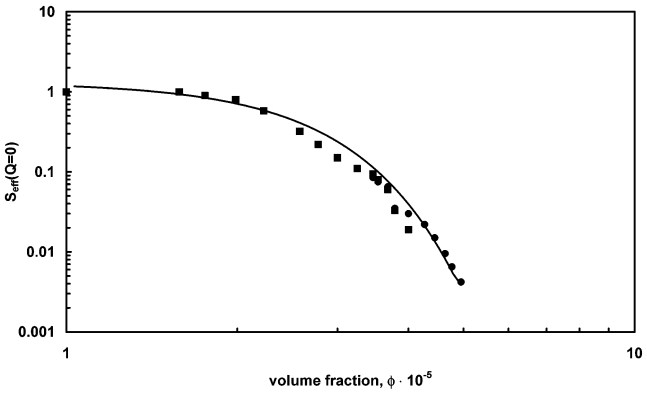

Figure 6. S_{eff} ($Q = 0$) obtained from static light scattering (■) and SAXS (●) in 1 mM NaCl (25 °C). The solid line represents the calculated form using the HNC approximation. Particle model, $\bar{a}$= 37.59 nm and particle charge, (756 ± 85)e.

but in this case, the significant difference between M_w and M_n may be due to the degree of polydispersity. By assuming a Gaussian distribution, values for the particle-size polydispersity, as determined for M_w and M_n, were found to be 0.19 for M_w and 0.23 for M_n, which are also higher than the value of 0.09 determined directly from the TEM particle-size distribution. Normally, osmotic pressure measurements do favor smaller particles, which could explain the low M_n value found here. Moreover, using a log-normal distribution, the particle-size polydispersity was recalculated from M_w and M_n and was found to be on the order of 0.14 for M_n and 0.12 for M_w. These values are also higher than those calculated from the particle-size measurements, so the difference can be attributed to the uncertainty in the values of M_w and particularly for M_n, which may give the impression of a much higher degree of polydispersity than actually exists in solution.

Furthermore, the ionic strength of the saline water was measured not only by conductivity but also by osmotic pressure measurements. Hence, a direct comparison can be made between the calculated and actual ionic strength. The measured osmotic pressure refers to that of the reservoir; this implies that, because of the Donnan phenomenon, the ionic strength of the lipid A dispersion is lower than in the actual solution containing lipid A. However, for the scattering experiments, dispersions of lipid A were made by dilution; therefore, the ionic strength should represent that of the dispersion containing lipid A.

Since for a given volume fraction ϕ particle interactions decrease with increasing ionic strength, eq 3 becomes significantly important as the osmotic pressure simultaneously decreases with increasing ionic strength at a salinity as low as 10 mM NaCl. Although the ionic strength at 10 mM NaCl may satisfy the conditions for weak interactions, the relatively low osmotic pressure values made precise measurements rather difficult. The osmotic pressure measurements normally have an error of ±2.1 Pa; therefore, a 15−25% degree of uncertainty in the dispersions at the lowest concentration of lipid A is associated with these measurements, which in turn influences the extrapolation for M_n.

C. Particle Surface Charge. The surface charge on the particles was determined by comparing $S_{eff}(0)$ obtained from LS experiments with those obtained from SAXS. The parameters used for this polydispersity model, specifically, the average particle size and the standard deviation of the particle size, are listed in Table 1. Table 2 lists the parameters employed for the HNC approximation for modeling $S(Q)$, where we applied 37.59 nm as the average particle radius, $\bar{\rho} = 0.078$, and the mole fractions of the three subcomponents. $I_p(Q)$ values were calculated from liquid-state theory, as was $S_{eff}(Q = 0)$. $S_{eff}(Q)$ was calculated from eq 15 with $I_{p,0}(Q)$ taken directly from the scattering intensity since it is assumed to be in the dilute concentration regime, which allows one to work in arbitrary units. For each volume fraction or concentration, $S_{eff}(Q = 0)$ was calculated by extrapolating the measured values of $S_{eff}(Q)$ to $Q = 0$. The measured $S_{eff}(Q)$ is the weighted sum of the partial structure factors, where each component of the polydisperse system is weighted by a factor of $x_i^{1/2} f_i(Q)$ (see Table 2), which scales for optically homogeneous spheres to the third power; hence, the largest contribution to $S_{eff}(Q)$ at low Q would arise from the largest particle. The effects of the intrinsic sample-size polydispersity are a broadening of the principal peak, a reduction in height, a shift of its position to lower wavenumbers, and a strong increase in its value at low Q. These influences have been examined by analyzing the contributions of each partial structure factor $S_{ij}(Q)$ of the subcomponent to the average structure factor $\bar{S}(Q)$.[33,34] Analyzing the data accordingly, we noticed no significant lowering or broadening of $S_{eff}(Q)$. Moreover, we see that the six $S_{ij}(Q)$ are not out of phase, hence supporting the low polydispersity in our samples and its insignificant influence on the principal peak. However, the width of $S_{eff}(Q)$ can also be affected by the charge polydispersity. Keeping the effective charge and volume fraction (ϕ_{fit}) fixed, we did not observe any significant changes in either the peak height or the position of $S_{eff}(Q)$ at small Q values. The absence of a decrease in peak height for $S_{eff}(Q = 0)$, where the other components do not contribute significantly to the scattered light, is another indication of the low polydispersity. The experimental and theoretical multicomponent results are shown in Figures 6−8. Figure 5 represents the $S_{eff}(Q = 0)$ results obtained from LS and SAXS as a function of volume fraction in comparison to theory using a particle radius of 37.59 nm, a particle charge of (756 ± 85)e, and an ionic strength of 1.0 mM NaCl. Figure 7 shows the dependency of $I_p(Q)$ on Q at various volume fractions of lipid A with the same parameters given in Figure 6. Figure 8 reveals the influence of the lipid A dispersions on ionic strength at 10.0 mM NaCl. The fitting procedure uses an average surface particle charge of (756 ± 85)e at an ionic strength of 10.0 mM NaCl (25 °C) whereas at very low ionic strength (1.0 mM) the ionic strength was taken from the conductivity and titration experiments and used in the calculation of $S(Q)$ and adjusted accordingly (2.75 mM). This discrepancy may be due to the release of bound sodium and chloride ions from the lipid A aggregate in the suspension and subsequently collected in the dialysate during the several changes of the dialysis procedure. However, increasing the volume fraction to $\phi \geq 3.75 \times 10^{-4}$ resulted in the formation of colloidal

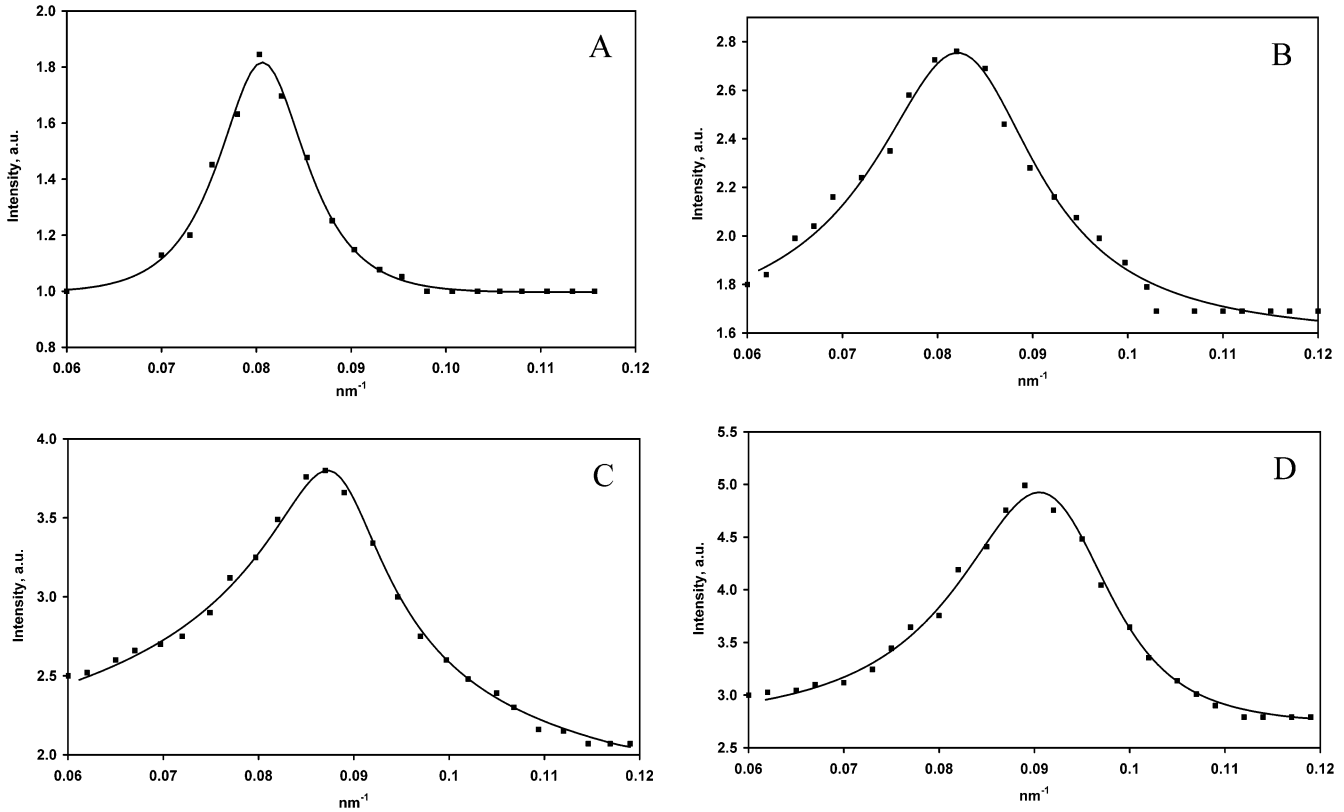

Figure 7. $I_p(Q)$ obtained and SAXS experiments vs Q (nm^{-1}) for lipid dispersions at various volume fractions: (D) $\phi = 3.75 \times 10^{-4}$; (C) $\phi = 3.50 \times 10^{-4}$; (B) $\phi = 2.50 \times 10^{-4}$; and (A) $\phi = 1.75 \times 10^{-4}$. The solid line represents the calculated parameters given in Figure 6, but at 1.0 mM NaCl and 25 °C.

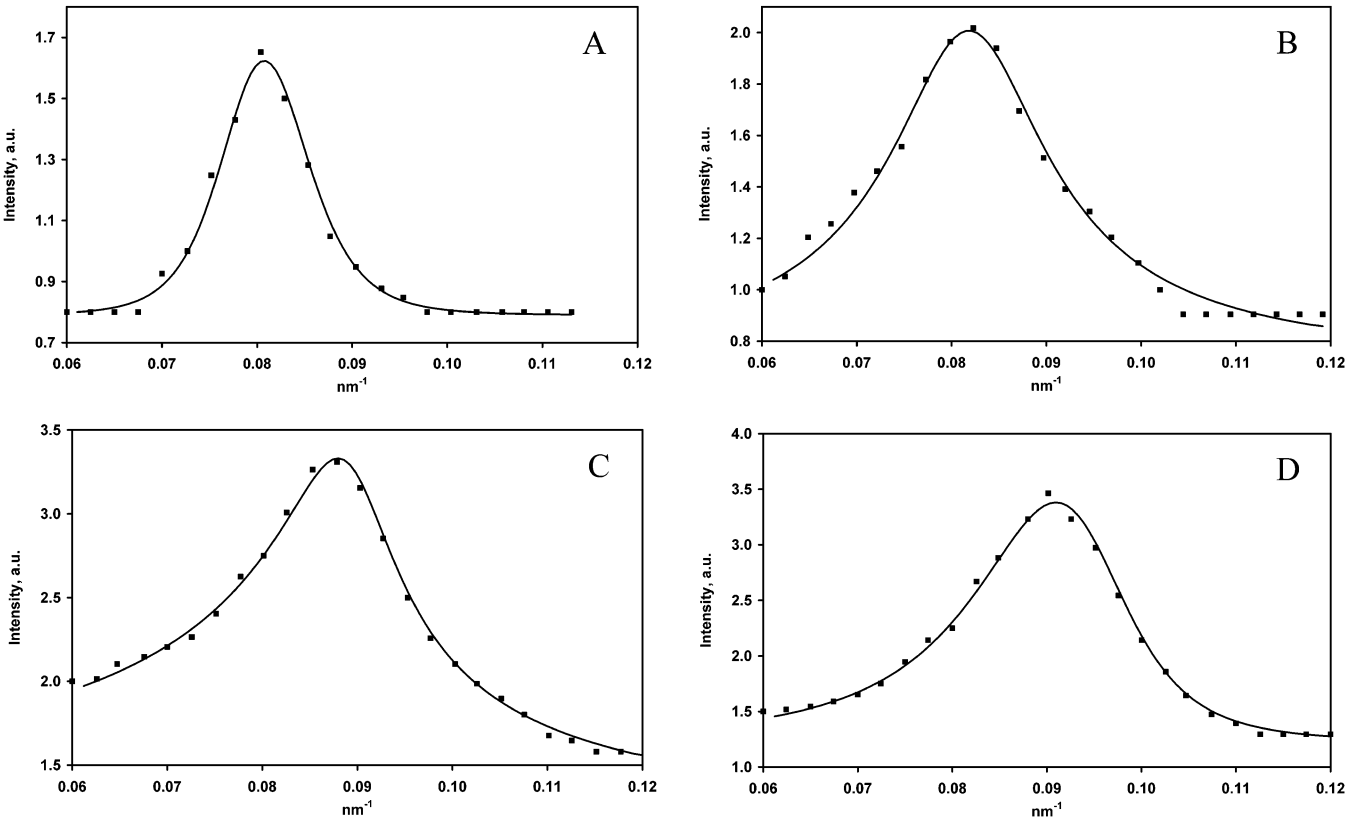

Figure 8. $I_p(Q)$ obtained from SAXS vs Q (nm^{-1}) for various volume fractions as in Figure 7, but at 10 mM NaCl (25 °C): (D) $\phi = 3.75 \times 10^{-4}$; (C) $\phi = 3.50 \times 10^{-4}$; (B) $\phi = 2.50 \times 10^{-4}$; and (A) $\phi = 1.75 \times 10^{-4}$. For the HNC approximation (—), the particle radius is $\bar{a} = 37.59$ nm, and the particle charge is (728 ± 34)e.

crystallization. Under the condition that 2.75 mM was used instead of 1.0 mM NaCl, the $S_{eff}(Q)$ values and the intensity distribution $I_p(Q)$ produced consistent and meaningful physical results, which could be extended up to a salinity of 15 mM

NaCl. Using the HNC approximation, the effective particle charge for lipid A was found to (756)e at 1.0 mM NaCl and (720)e at 10 mM NaCl, respectively. The fitting procedure of the scattering spectra to determine the particle charge is not straightforward.[30] The DLVO expression (eq 17) implicates a linearization of colloid−colloid interactions, so a renormalization of charge (postcondensation) has to be performed, which is smaller than the structural charge. We applied the approach by Alexander et al.[36] based on the Poisson−Boltzmann cell model (PBC). Using these criteria, we found that if (756)e is taken as the actual structural particle charge then the effective particle charge for the linearized Poisson−Boltzmann charge is (410)e at 1.0 mM NaCl and (455)e at 10.0 mM NaCl. Moreover, preliminary results obtained from static light-scattering measurements and titration experiments similar to those in ref 3 yielded a total surface-charge density of $\rho_T = 0.28$ C/m^2, a pK_a of 4.35, a Stern capacity of $C_s = 0.62$F/m^2, and an α_{diss} value of 3.59×10^{-2}. These values are consistent with the view that, assuming all sites of the colloidal lipid A were charged, the number of surface charges would be 2650 sites per particle. However, the large discrepancy between the number of total sites (2650) and the structural colloidal charge of 756e indicates that only a small fraction of the sites are in fact ionized.

D. Osmotic Pressure and Structure Factor in the $Q \rightarrow 0$ Limit. Despite the degree of polydispersity in this system at low ionic strength (25 °C), the directly measured osmotic pressure was compared to that calculated from the structure factor data by applying eqs 7 and 9, even though there is some lack of validity due to the polydispersity. The effect of the size polydispersity, although found to be small, is to broaden the principal peak of $S(Q)$, reduce its height, slightly shift the position to smaller Q values, and significantly increasing the value at small Q because of the contribution of the partial $S_{ij}(Q)$ to the average $\bar{S}_{eff}(Q)$.[33] Therefore, we replaced $S(O = 0)$ with $S_{eff}(Q = 0)$ for all lipid A dispersions and plotted the values obtained on a semilog plot that, to some extent, eliminates the discrepancies (Figure 8). The agreement between theory and experiment, LS and SAXS, is surprisingly good, which justifies the use of eqs 7 and 16. The consistency between the directly obtained results and the indirectly measured osmotic pressures justifies the assumptions made above. It seems that eq 7 may be useful for systems that are not really monodisperse or that, for charged particles, a higher degree of polydispersity can be tolerated. For an electrostatically stabilized system that is considered to consist of hard spheres, it can be anticipated that diffuse ionic clouds will surround the lipid A particles and will subsequently interact long before the lipid A particles come into close contact. However, LS and SAXS results reveal an uncertainty in the measured osmotic pressures at low volume fractions. The calculated osmotic pressures from LS and SAXS are in good agreement at moderate volume fractions between $2.5 \times 10^{-4} < \phi < 3.5 \times 10^{-4}$; this is not so for volume fractions between $1.5 \times 10^{-4} < \phi < 2.19 \times 10^{-4}$. For such a system (e.g., lipid A) and by taking the experimental uncertainties associated with the different experiments into account assuming a monodisperse system, we would expect that, with increasing volume fraction, the discrepancy would be greater at high volume fractions, but the opposite appears to be the case. For ionic strengths of both 1.0 and 10.0 mM NaCl (Figure 9A and B), it seems that for the lipid A dispersions the osmotic pressures at the limit $\phi \rightarrow 0$ are lower than those predicted from direct measurements. This would result in a higher value of $\overline{M_n}$, which more closely approximates to $\overline{M_w}$ and subsequently results in a lower degree of polydispersity.

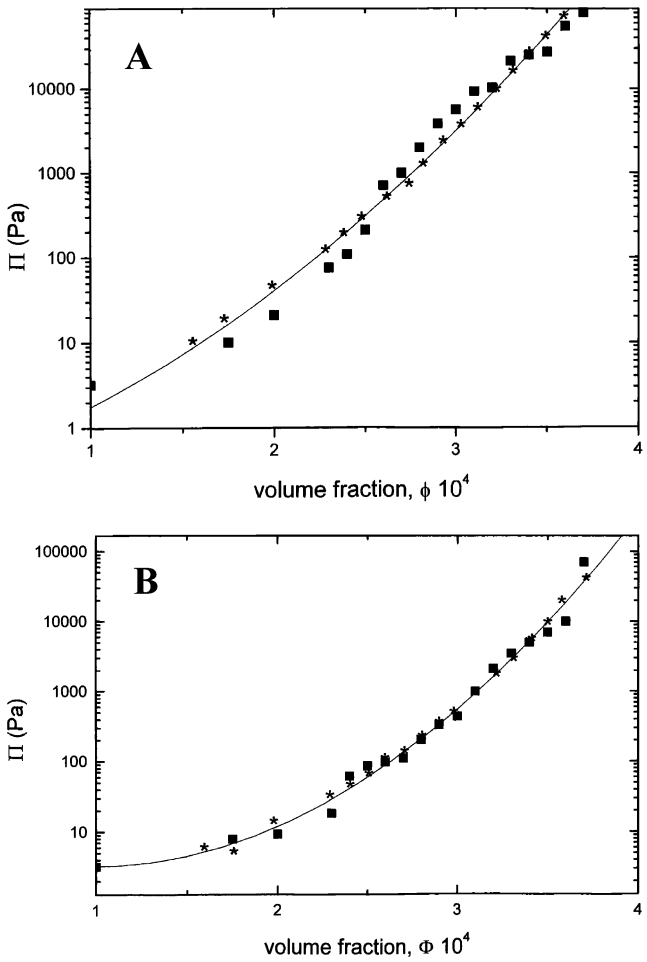

Figure 9. (A) Comparison of the experimentally determined osmotic pressure of lipid A dispersions at 10.0 mM NaCl with the calculated ones with the experimental $S_{eff}(Q = 0)$ values determined from static light scattering (■) and from SAXS (*). (B) The same as in A but at 1.0 mM NaCl.

We have attempted to model the osmotic pressure through the PBC model[36,37] and the multicomponent model using the HNC approximation. In the PBC model, each colloidal particle is arranged at the center of a spherical cell, the ionic distribution in the cell is calculated by using a nonlinearized Poisson−Boltzmann equation,[38] and the pressure is determined from the total ionic concentration at the edge of the cell according to Marcus.[39] The effective charge for lipid A was (765)e, and the ionic strengths that were applied were 2.54 and 9.23 mM NaCl (25 °C).[40] The osmotic pressure data are reasonably well represented only by the BPC model for an ionic strength of 10 mM, although the fit is not perfect (Figure 10) when the quality of the osmotic pressure is taken into account, particularly at dilute solutions. One reason for the lack of a reasonable fit is the vanishing second virial coefficient. Since each particle is positioned in the center of a cell, the interparticle force is zero, although the ions are treated correctly. Surprisingly, the osmotic pressure data are satisfactorily modeled in the volume-fraction range of $2.20 \times 10^{-4} < \phi < 3.00 \times 10^{-4}$ but less so for the HNC approximation using the multicomponent model. We can currently offer no explanation for this unless the experimental data are so reliable in this volume-fraction range that volume concentration, ionic strengths, and temperature ideally fit the theory.

E. Crystallization and Structure. For volume fractions of lipid A dispersions in the range of $3.50 \times 10^{-4} < \phi < 5.15 \times 10^{-4}$ and at 1.0 mM NaCl (8−10 °C), the formation of colloidal

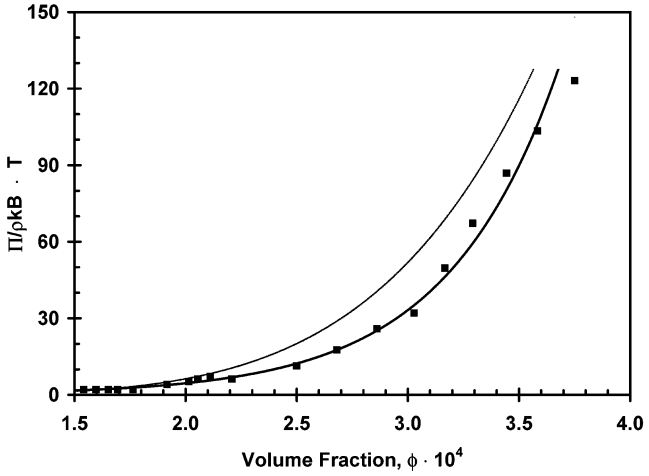

Figure 10. Comparison of the osmotic pressure measurements at 10.0 mM NaCl ionic strength applying the PBC model (—) and the multicomponent HNC approximation (- -).

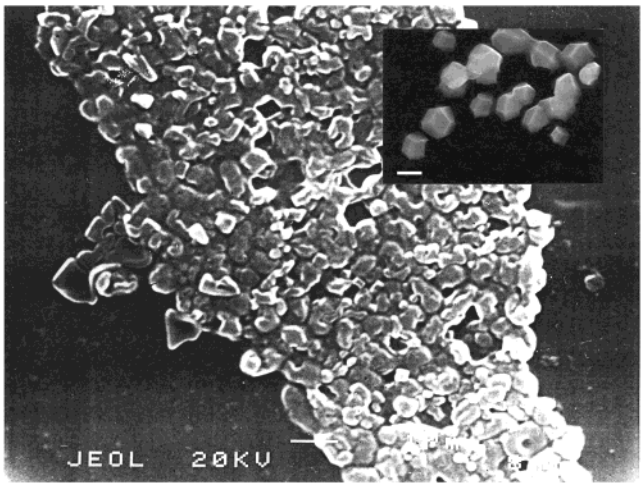

Figure 11. SEM picture of colloidal crystals of lipid A (diphosphate), $\phi = 4.25 \times 10^{-4}$ Inset: Selected area of colloidal crystals of lipid A (diphosphate). The bar equals 2.0 μm.

crystals can be observed (Figure 11). The solution is still transparent to light, and the transparency does not change upon gradually increasing the ionic strength to 10 mM NaCl; however, the solution becomes iridescent upon standing for 5 to 6 weeks because of the formation of large colloidal crystals ($\sim$1$-$2 μm). No iridescence was observed with further increases in the volume fraction in 1 mM NaCl or lower concentrations (i.e., in the absence of salt). These transparent solutions at moderate volume fraction ($3.50 \times 10^{-4} < \phi < 4.15 \times 10^{-4}$) as well as the ones at high volume fraction ($4.15 \times 10^{-4} < \phi < 5.15 \times 10^{-4}$) in the presence of 1 and 10 mM NaCl, respectively, have been analyzed by SAXS and LS.

At high volume fraction ($4.15 \times 10^{-4} < \phi < 5.15 \times 10^{-4}$) and both ionic strengths (1.0 and 10.0 mM NaCl), the X-ray spectra indicate the presence of long-range order (Figure 12). The assignments of the respective peaks to the crystal planes were made from comparisons of the observed peak vectors according to eq 18:

$$Q_{hkl} = \frac{2\pi}{a}(h^2 + k^2 + l^2)^{1/2} \qquad (18)$$

where h, k, and l are the Miller indices and a is the unit-cell size. The observed peaks were found to be reflections originating from a face-centered cubic (fcc) lattice with a unit-cell dimen-

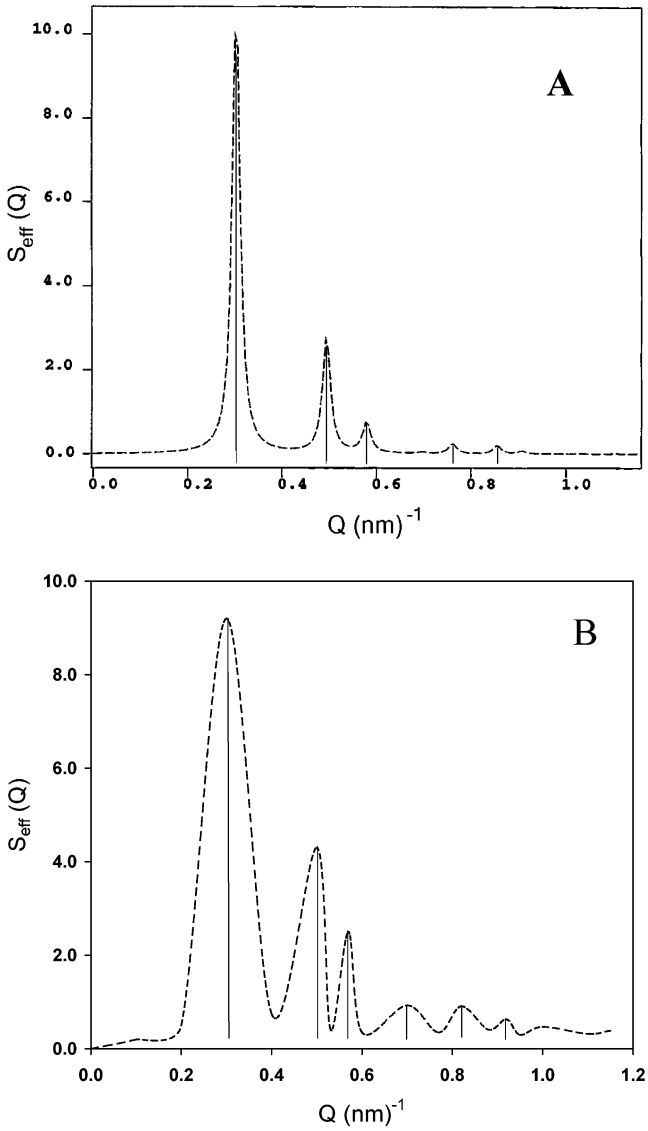

Figure 12. (A) Light-scattering spectra, $S_{eff}(Q)$ vs Q, obtained from lipid A dispersions at a volume fraction of $\phi = 4.75 \times 10^{-4}$ and 1.0 mM NaCl. The peak positions are assumed to be from a fcc-type structure.[40] (B) SAXS spectra, $S_{eff}(Q)$ vs Q, for the same sample of lipid A (diphosphate).

sion of $a = 57.25 \pm 1.5$ nm.[40] The Bragg distances observed from the Q values using the Bragg equation $d = 2\pi/Q$ agreed with the corresponding values calculated from the sphere concentration. Because of the very few diffraction lines observed in the X-ray spectrum, it was not possible to determine the space group unequivocally. Upon increasing the volume fraction, no additional higher-order peaks were found in the spectra; this strongly suggests that an ordered structure is present under this condition. The indication of long-range-order behavior of lipid A suspensions suggests that the degree of polydispersity associated with this charged system is tolerated. Pusey[41] calculated for hard spheres that the degree of polydispersity where colloidal crystals appear did not exceed 0.07$-$0.11, but for the almost negligible effect of the determined polydispersity (QELS) on the mean-square displacement for the large interactions, we can assume that the time to form these structures of lipid A is not dominated by the degree of polydispersity It can be inferred that the increase in time in forming these colloidal crystals increases the degree of polydispersity.

The formation of colloidal crystals at volume fractions of $3.75 \times 10^{-4} < \phi < 4.15 \times 10^{-4}$ in the presence of 1.0 mM

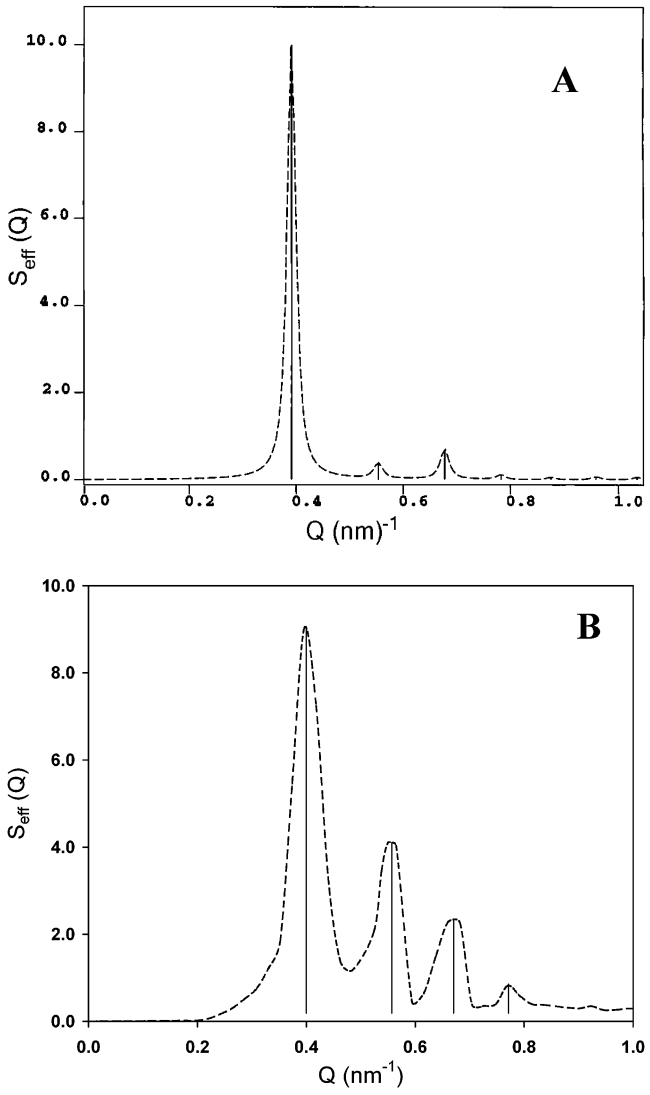

Figure 13. (A) Light-scattering spectra, $S_{eff}(Q)$ vs Q, obtained from free lipid A dispersions at a volume fraction of $\phi = 4.05 \times 10^{-4}$ and 1.0 mM NaCl. The peak positions are assumed to be from a bcc-type structure. (B) SAXS spectra, $S_{eff}(Q)$ vs Q, for the same sample of lipid A (diphosphate).

NaCl, where no iridescence is observed, has also been analyzed by SAXS. Within this volume-fraction regime, the presence of long-range order can also be seen, but surprisingly, the diffraction peaks are at different positions (Figure 14). This X-ray spectrum was indexed on the basis of a bcc lattice with $a = 36.14 \pm 1.3$ nm. From the X-ray spectra obtained at 1 mM NaCl and $\phi = 4.05 \times 10^{-4}$, it was assumed that the first peak corresponds to that of the closest-packed plane in the bcc structure (i.e., (110) having a spacing of 0.2458 nm^{-1}). Assuming that this first peak corresponds to the (110) plane, $d = d_{110}$. Since there should be two molecules per unit cell for a bcc lattice and the concentration of lipid A is known, the molecular weight can be calculated according to eq 19:

$$\mathrm{MW} = (\sqrt{2})d_{110})^{1/3}\left(\frac{c}{2}\right) \qquad (19)$$

From eq 19, we calculated a molecular weight of 10.05×10^6 g/mol, which is consistent with the value found from LS and osmotic pressure experiments reported earlier. These two colloidal crystal forms appear to be in equilibrium. Increasing the liquid phase with lipid A at constant low ionic strength (1 mM or lower) results in the formation of an fcc lattice in addition to the bcc lattice originally found. The diffraction lines are clearly distinguishable for both structures. If the concentration of the liquid phase of lipid A was kept constant ($\phi \cong 3.9 \times 10^{-4}$), then after 4 weeks most of the colloidal crystals transformed to the fcc structure with approximately 7% admixed bcc structure. Under other conditions, significant fractions of the fcc structure and the bcc structure were present simultaneously (Figure 14).

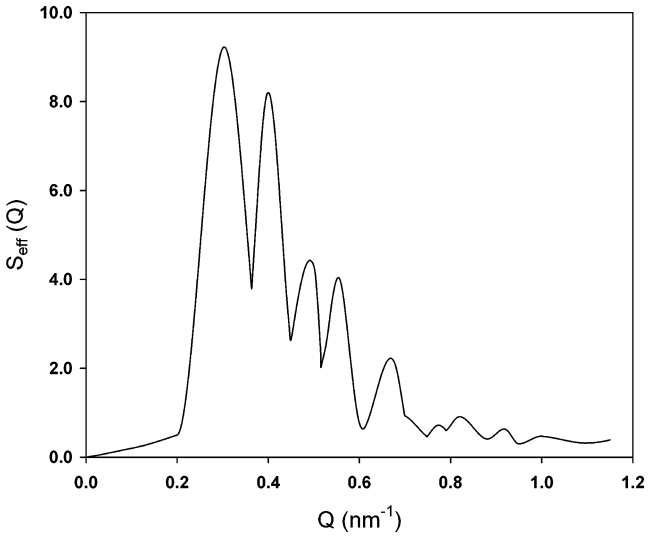

Figure 14. SAXS spectra, $S_{eff}(Q)$ vs Q, obtained from lipid A (diphosphate) dispersions at a volume fraction of $\phi = 4.05 \times 10^{-4}$ and 1.0 mM NaCl obtained after 14 days showing both bcc and fcc structures.

It is noteworthy that the quality of the diffraction data is strongly related to the sizes of the colloidal crystals of lipid A grown under deionized conditions. The relative intensity distributions (Figures 12 and 13) of the calculated and observed Bragg reflections, particularly those of the weak ones compared to the first-order *hkl* Bragg reflections (e.g., (110) or (111)) are sensitive to variations in the size of these colloidal crystals. The ultimate size and shape of the colloidal crystal form of the lipid A aggregate will determine the geometrical arrangement. For example, they may have rounded, spherical, or ellipsoid or facetted shapes (hexagonal in shape) or form small cubic crystals, all of which have been observed in electron micrographs (TEM, SEM; see Figure 11 inset). The presence or absence of any of these forms in the colloids cannot be currently established.

The Q dependence ($0.1 \leq Q/Q_{110} \leq 0.75$) of the scattering of the liquid phase and the crystalline bcc phase are very similar (i.e., the peak in $S(Q)$ for the liquid is close to $Q = Q_{110}$). This suggests a similarity in the structure of the liquid and the bcc crystal phase. If we assume that the bcc structure Q_{110} generates the first peak in $S(Q)$, then we would expect a second peak to be located at $Q = \sqrt{2}Q_{110}$. However, we notice the first minimum in $S(Q)$ in the liquid state. Although we observe higher orders in the bcc structure, we see only a shallow peak in the liquid structure factor at $Q = 1.67Q_{110}$, which is an indication that the wavevector dependence of the liquid dispersion of lipid A has some features in common with that for the longitudinal (110) lattice vibrations in the bcc crystal.[42]

It has been demonstrated by a number of authors[43−45] that bcc lattices are seen for systems that interact via long-ranged interactions, and this seems to be particularly true at low ionic strengths. However, this system at 10 mM NaCl seems to be closer in behavior to hard spheres whereas this is not true for

the system at 1 mM NaCl, which behaves as ionic particles. Perhaps such a system is sensitive toward the degree of polydispersity, and the observed degree of polydispersity may be one reason for the inhibition of the formation of long-range fcc order resulting in the formation of a bcc lattice. Furthermore, a very recent contribution by van Roi and Hansen[46] has shown theoretically the possible coexistence of fluid-fcc and fluid-bcc structures at very low ionic strength. This arises because the free-energy difference between fcc and bcc is much smaller than for the fluid, and it is not possible to distinguish between fcc or bcc precisely. It is most likely, therefore, that the observations reported here are due to the existence of long-lived metastable colloidal crystallites at very low ionic strength.[47]

V. Conclusions

The physical characterization of an aqueous and transparent lipid A dispersion over a wide range of volume fractions has been carried out by applying LS, SAXS, and osmotic pressure experiments in addition to SEM and TEM measurements. Although the effects of the degree of polydispersity cannot be ignored, excellent agreement was found between the directly measured osmotic pressure and that indirectly established from the scattering data at zero-angle scattering by applying liquid-state theory. Liquid-state theory has also been used to calculate the surface charge of the lipid A dispersion using the scattered intensities. The fit of both $S_{\text{eff}}(Q = 0)$ and the prominent peak for $I_{\text{p}}(Q)$ with the same particle charge is in support of the main conclusions drawn from these experiments. This is especially important because interparticle interactions and the degree of polydispersity have a major influence on the limit of zero-angle scattering.

In addition, by raising the volume fraction of lipid A at low salinity (1 mM), it has been possible to detect two ordered structures in solution. The observed colloidal crystal lattices apparently can be transformed from an fcc subphase to a bcc lattice when the "sphere" concentration of lipid A molecules decreases in the presence of 1−10 mM salt.

Acknowledgment. Dipl.-Ing. P. Quitschau acknowledges financial support from the Biomaterials Project, Brussels (BMH4-CT 96-0013). We acknowledge Professors D. K. Ross and S. E. Donnelly and Dr. N. M. Boag for their support, encouragement, and discussions and Dipl-.Ing. H. Reichelt for printing the figures.

References and Notes

(1) (a) Quesada-Perez, M.; Callejas-Fernandez, J. R.; Hidalgo-Alvarez, R. *Adv. Surf. Interface Sci.* **2002**, *95*, 295. (b) *New Approaches to Problems in Liquid State Theory: Inhomogenieties and Phase Separation in Simple, Complex, and Quantum Fluids*; Cacamo, C., Hansen, J.-P., Stell, G., Eds.; NATO Science Series, Series C, Mathematical and Physical Sciences; Kluwer Academic Publishers: Dordrecht, The Netherlands, 1999; Vol. 529. (c) Porn, W.; Pusey, P. N.; Lekkerkerker, H. *Phys. World* **1996**, *9*, 27. (d) Crocker, J. C.; Grier, D. G. *Phys. Rev. Lett*. **1994**, *73*, 352. (e) Crocker, J. C.; Grier, D. G. *MRS Bull.* **1998**, *23*, 24. (f) Genz, U.; D'Aguanno, B. G.; Mewis, J.; Klein, R. *Langmuir* **1994**, *10*, 2206. (g) van Roij, R. *J. Phys.: Condens. Matter* **2000**, *12*, 263.

(2) Chang, J.; Lesieur, P.; Delsanti, M.; Belloni, L.; Bonnet-Gonnet, C.; Cabane, B. *J. Phys. Chem.* **1995**, *99*, 15993.

(3) Thies, M.; Quitschau, P.; Zimmermann, K.; Rusch, V.; Faunce, C. A.; Paradies, H. H. *J. Chem. Phys.* **2002**, *116*, 3471.

(4) Persello, J.; Magnin, A.; Chang, J.; Piau, J. M.; Cabane, B. *J. Rheol.* **1994**, *38*, 1.

(5) (a) Hiltner, P. A.; Krieger, I. M. *J. Phys. Chem.* **1969**, *73*, 2386. (b) Monovoukas, Y.; Gast, A. P. *Langmuir* **1991**, *7*, 460. (c) van Bladeren, A. *MRS Bull.* **1998**, *23*, 39. (d) Schmitz, K. S. *Phys. Chem. Chem. Phys.* **1999**, *1*, 2109.

(6) (a) Fereira, P. G.; Dimitrowska, M.; Belloni, L. *J. Chem. Phys.* **2000**, *113*, 9849. (b) Mendez-Alcaraz, J. M.; Klein, R. *Phys. Rev. E* **2000**, *61*, 4095. (c) Dinsmore, A. D.; Yodh, A. G.; Pine, D. J. J. *Phys. Rev. E* **1995**, *52*, 4045. (d) Tohver, V.; Chan, A.; Sakurada, O.; Lewis, L. A. *Langmuir* **2001**, *17*, 8414.

(7) Garibay-Alonso, R.; Mendez-Alcaraz, J. M.; Klein, R. *Physica A* **1997**, *235*, 159.

(8) Raetz, C. R. H.; Whitfield, C. *Annu. Rev. Biochem.* **2002**, *71*, 635. Note: The release of endotoxin is intimately associated with septic shock. This problem caused more than 21 000 mortalities in 1996 in the U.S. alone. *Morb. Mort. Wkkly. Rep.* **1997**, *46*, 941−944 (Centers for Disease Control and Prevention, Atlanta, GA).

(9) (a) Ribi, E. E.; Cantrell, J. L.; van Eschen, K. B.; Schwartzmann, S. M. *Cancer Res.* **1979**, *39*, 4756. (b) Takayama, K.; Quereshi, N.; Ribi, E. E.; Cantrell, J. L. *Rev. Infect. Dis.* **1984**, *6*, 439. (c) Glauser, M. P.; Zanetti, G.; Baumgartner, J.-G.; Cohen, J. *Lancet* **1991**, *338*, 732.

(10) Kotra, L. R.; Golemi, D.; Amoro, N. A.; Liu, G.-J.; Mohasbery, S. *J. Am. Chem. Soc*. **1999**, *121*, 807.

(11) (a) Raetz, C. R. In *Escherichai coli and Salmonella: Cellular and Molecular Biology*, 2nd ed; ASM Press: Washington, DC, 1996; Vol. 1, p 1035. (b) Paradies, H. H.; Rusch, V.; Zimmermann, K. U.S. Patent Application No. 60/263,494, 2002, pending.

(12) (a) Hauser, P.; Voet, P.; Sloani, M.; Garcon-Johnson, N. M.-J.; Desmond, P. U.S. Patent 5,776,468, 1998. (b) Alving, C. R. *Immunobiology* **1993**, *187*, 430.

(13) (a) Hayashida, O.; Kato, M.; Akaiyi, K.; Aoyama, Y. *J. Am. Chem. Soc*. **1999**, *121*, 11587. (b) Li, C.; Budge, L. P.; Driscoll, C. D.; Willardson, B. W.; Allman, G. W.; Savage, P. B. *J. Am. Chem. Soc*. **1999**, *121*, 931.

(14) (a) Amor, K.; Heinrichs, D. E.; Friedrich, E.; Ziebel, K.; Johson, R. P.; Whitflield, C. *Infect. Immun.* **2000**, *68*, 116. (b) Thieblemont, N.; Thieringer, R.; Wright, S. D. *Immunity* **1998**, *8*, 771.

(15) Chan, S.; Horner, S. R.; Fauchet, P. M.; Miller, B. J. *J. Am. Chem. Soc.* **2001**, *123*, 11797.

(16) (a) Archibald, D. A.; Mann, S. *Nature (London)* **1993**, *364*, 430. (b) Paradies, H. H.; Thies, M.; Hinze, U. *Rigaku J.* **2000**, *17*, 9.

(17) Faunce, C. A.; Quitschau, P.; Thies, M.; Scheidt, T.; Paradies, H. H. *Bacteria & Bacterial Fragments as Immunomodulatory Agents;* Old Herborn University Seminar on Probiotics; Herborn Litterae: Herborn, FRG, 2002; Vol. 15, pp 95−120.

(18) Evans, D. F.; Wennerstrom, H. A. *The Colloidal Domain: Where Physics, Chemistry, Biology and Technology Meet;* VCH Publishers: New York, 1994.

(19) (a) Russel, W. B.; Saville, D. A.; Schowalter, W. R. *Colloidal Dispersions*; Cambridge University Press: Cambridge, U.K., 1995. (b) Murray, C.; Sprenger, W.; Seshadri, R.; Cerise, J. *Mater. Res. Soc. Symp. Proc.* **1995**, *366*, 163.

(20) Scheidt, T.; Hinze, U.; Quitschau, P.; Paradies, H. H. *4th Microbial Induced Corrosion*; Sequeira, C, Tiller, K., Eds.; Materials Institute: London, 2000; pp 140−169.

(21) Coughlin, R. T.; Tonsager, S.; McGroarty, E. J. *Biochemistry* **1983**, *22*, 2002.

(22) Bartlett, M. J. *J. Biol. Chem.* **1959**, *234*, 466.

(23) Hayter, B. J.; Rivera, M.; McGroarty, E. J. *J. Biol. Chem.* **1987**, *262*, 5100.

(24) Hannecart-Pokorni, E.; Dekegel, E.; Satterthwait, A. C. *Eur. J. Biochem.* **1973**, *38*, 6.

(25) Shands, J. W., Jr.; Chun, W. *J. Biol. Chem*. **1980**, *255*, 1221.

(26) Kim, S. H.; Cotts, P. M. *J. Appl. Polym. Sci.* **1991**, *42*, 217.

(27) Guinier, A. *Small-Angle Scattering of X-rays;* Wiley: New York, 1955.

(28) (a) Paradies, H. H. *Colloids Surf.* **1993**, *74*, 57. (b) Clancy, S. F.; Paradies, H. H. *Z. Phys. Chem. (Munich)* **2001**, *215*, 4, 483.

(29) (a) Clancy, S. F.; Tanner, D. A.; Steiger, P. H.; Thies, M.; Paradies, H. H. *J. Phys. Chem.* **1994**, *98*, 11143. (b) Paradies, H. H.; Clancy, S. F.; Thies, M. *J. Phys. Chem.* **1996**, *100*, 9881.

(30) (a) Hansen, J.-P.; McDonald, L. R. *Theory of Simple Liquids;* Academic Press: New York, 1976. (b) Belloni, L. *J. Chem. Phys*. **1986**, *85*, 519. (c) Belloni, L. *Chem. Phys*. **1993**, *98*, 8080. (d) Gisler, T.; Schultz, F.; Barkovec, M.; Sticker, H.; Schurtenberger, P.; D'Aguanno, B. G.; Klein, R. *J. Chem. Phys.* **1994**, *101*, 9924.

(31) Rogers, F. J.; Young, D. A. *Phys. Rev. A* **1984**, *30*, 999.

(32) Verwey, E. J. W.; Overbeck, J. Th. G. *Theory of the Stability of Hydrophobic Colloids;* Elsevier: New York, 1948.

(33) (a) D'Aguanno, G. D.; Klein, R. *J. Chem. Soc., Faraday Trans.* **1991**, *87*, 379. (b) D'Aguanno, G. D.; Klein, R. *Phys. Rev. A* **1992**, *46*, 7652.

(34) (a) Phalakornkul, J. K.; Gast, A. P.; Pecora, R. *Phys. Rev. E* **1996**, *54*, 661. (b) Nägele, G.; Kellerbauer, O.; Krause, R.; Klein, R. *Phys. Rev. E* **1993**, *47*, 2662. (c) Wagner, N. J.; Krause, R.; Rennie, A. R.; D'Aguanno, B. G.; Goddwin, J. *J. Chem. Phys.* **1991**, *5*, 494.

(35) Pusey, P. N. In *Liquids, Freezing and Glass Transitions;* Hansen, J.-P., Levesque, D., Zimm-Justin, L., Eds.; North-Holland: Amsterdam, 1980.

(36) Alexander, S.; Chaikin, P. M.; Grant, P.; Morales, G. J.; Pincus, P. *J. Chem. Phys*. **1984**, *80*, 5776.

(37) (a) Belloni, L. *Chem. Phys*. **1988**, *88*, 5143. (b) Belloni, L. *J. Chem. Phys.* **1993**, *98*, 8080. (c) Belloni, L.; Drifford, M.; Turq, P. *J. Chem. Phys*. **1984**, *83*, 147.

(38) Bell, G. M.; Dunning, A. J. *Trans. Faraday Soc.* **1970**, *66*, 500.

(39) Marcus, R. A. *J. Chem. Phys.* **1955**, *23*, 1057.

(40) From neutron scattering experiments at the Institute von Laue-Langevin, Grenoble, France, using the D-11 beam line, $a = 55.75 \pm 3.5$ nm was determined (Brown, H.; Ross, K. D.; Paradies, H. H.; May, R. Unpublished work, September 2001).

(41) Pusey, P. N.; van Megen, W.; Underwood, S. M. *J. Chem. Soc., Faraday Trans.* **1991**, *87*, 395.

(42) Cotter, L. R.; Clark, N. A. *J. Chem. Phys.* **1987**, *86*, 6616.

(43) Monovoukas, Y.; Gast, A. B. *J. Colloid Interface Sci.* **1989**, *128*, 533.

(44) Okubo T. In *Phase Diagram of Ionic Colloidal Crystals;* Schmitz, K. S., Ed; ACS Symposium Series 548; American Chemical Society: Washington, DC, 1994; pp 364−380.

(45) Sirota, E. B.; Ou-Yang, H. D.; Sinha, S. K.; Chaikin, P. M. *Phys. Rev. Lett.* **1982**, *62*, 1524.

(46) van Roij, R.; Hansen, J.-P. *Phys. Rev. Lett*. **1997**, *79*, 3082.

(47) Larsen, A. E.; Grier, D. G. *Nature (London)* **1997**, *385*, 230.